crystals

MDPI

Article

4-Methyl/Phenyl-1,2,5,6-tetraazafluoranthen-3(2*H*)-ones Synthesis: Mechanistic Pathway Study and Single-Crystal X-ray Analysis of the Intermediates

Ahmed A. M. Sarhan [1], Matti Haukka [2], Assem Barakat [3,*], Saied M. Soliman [4], Ahmed T. A. Boraei [5,*], Manar Sopaih [5] and Eid E. Salama [5]

[1] Chemistry Department, Faculty of Science, Arish University, Al-Arish 45511, Egypt; asarhan@aru.edu.eg
[2] Department of Chemistry, University of Jyväskylä, P.O. Box 35, 40014 Jyväskylä, Finland; matti.o.haukka@jyu.fi
[3] Department of Chemistry, College of Science, King Saud University, P.O. Box 2455, Riyadh 11451, Saudi Arabia
[4] Chemistry Department, Faculty of Science, Alexandria University, P.O. Box 426, Alexandria 21321, Egypt; saeed.soliman@alexu.edu.eg
[5] Chemistry Department, Faculty of Science, Suez Canal University, Ismailia 41522, Egypt; manar_shalabi@science.edu.eg (M.S.); eidsalama2000@gmail.com or eid_mohamed@science.suez.edu.eg (E.E.S.)
* Correspondence: ambarakat@ksu.edu.sa (A.B.); ahmed_tawfeek83@yahoo.com or ahmed_boraei@science.suez.edu.eg (A.T.A.B.); Tel.: +966-11467-5901 (A.B.); Fax: +966-11467-5992 (A.B.)

Abstract: The synthesis of 4-methyl/phenyl-1,2,5,6-tetraazafluoranthen-3(2*H*)-one **4** and **7** has been reported with ninhydrin via a reaction first with ethyl acetoacetate or ethyl benzoylacetate and then a reaction of the resultant esters with hydrazine hydrate. The mechanism of hydrazinolysis and cyclization to obtain tetraazafluoranthen-3(2*H*)-ones is ambiguous, and the previously proposed mechanism was not based on facts because the actual intermediates were not isolated. Herein, the important intermediates involved in the hydrazinolysis–cyclization mechanistic pathway were isolated and characterized using NMR and X-ray single-crystal analysis. The intermediates demonstrate that the reaction carried out via two hydrazinolysis–cyclization reactions, the first of which includes the condensation of one hydrazine molecule with two ketone groups and the second of which includes the reaction of another hydrazine molecule with the ester and then condensation with the other ketone group. The stability of hydrazide **11** enabled the hydrazine to reduce the carbonyl of the ketone group to form **12** via a Wolff–Kishner-like reduction. The structure of the three intermediates was confirmed using X-ray crystallographic analysis. It was found that the three fused ring systems deviated from planarity to different extents, with their deviation from being coplanar reaching up to 5.3°. The possible non-covalent interactions which control the molecular packing of these intermediates were elucidated with the aid of Hirshfeld analysis.

Keywords: single-crystal X-ray; tetraazafluoranthen-3(2*H*)-one; reaction mechanism; Hirshfeld surface analysis

Citation: Sarhan, A.A.M.; Haukka, M.; Barakat, A.; Soliman, S.M.; Boraei, A.T.A.; Sopaih, M.; Salama, E.E. 4-Methyl/Phenyl-1,2,5,6-tetraazafluoranthen-3(2*H*)-ones Synthesis: Mechanistic Pathway Study and Single-Crystal X-ray Analysis of the Intermediates. *Crystals* **2023**, *13*, 1537. https://doi.org/10.3390/cryst13111537

Academic Editor: Ana M. Garcia-Deibe

Received: 9 October 2023
Revised: 18 October 2023
Accepted: 24 October 2023
Published: 26 October 2023

1. Introduction

A unique class of polycyclic aromatic chemical substances with potential applications is the fluoranthenes (Benzo[j,k]fluorene), which consist of four fused aromatic heterocycles [1–4]. Fluoranthenes have garnered a lot of interest due to their distinctive optoelectronic characteristics and wide range of applications [5]. Despite the development of numerous synthetic techniques for the production of fluoranthene derivatives, their relatively low reactivity and selectivity make it difficult to functionalize the fluoranthene structure at various positions [6].

A fluoranthene is a precursor structural component of many naturally occurring fungal compounds, for example, daldinone E (fungus Daldinia sp.) [7] and hortein [8].

Additionally, FLUN-550, a fluoranthene-based fluorescent probe for targeted labeling of intracellular lipid droplets, was introduced. Fluoranthenes' synthesis and modification have recently attracted a lot of attention. The most widely utilized strategies for their synthesis are the Diels–Alder reaction [9–12] and reactions that are catalyzed by transition metals [13–24]. As the fluoranthene skeleton is a structure that is frequently present in both fluorescent materials and natural products, it is of the utmost importance to investigate for the development of an effective, straightforward approach for diversity-oriented fluoranthene synthesis. However, current synthetic techniques call for harsh reaction conditions, substrates with a confined application range, or both [25].

The majority of reported fluoranthenes have been produced using arylboronic acids and 1,8-dichloronaphthalenes in the presence of $Pd_2(dba)_3$ as a catalyst at high temperatures (155–175 °C). Fluoranthenes can be created through inter- and intramolecular C-H arylation. Selectively substituted fluoranthenes were produced through the Suzuki–Miyaura reaction [26,27].

Koutentis et al. used both oxidative and nonoxidative cyclization methodology to create fluoranthene aza derivatives [28]. In other methods, silica sulfuric acid has been used as a reused solid catalyst for the one-pot synthesis of densely substituted pyrrole-fused isocoumarins [29]. Azafluoranthenes have been synthesized through the reaction of 8-(alkynyl)-1-naphthaldehydes and isocyanoacetates via aldol condensation/[1 + 2 + 3]. By using widely available starting components, domino reaction promotes the sequential synthesis of three new bonds and two rings in a single step. Additionally, this process can be used to create benzo[c][2,6]naphthyridines and chromeno[4,3-c]pyridines in mild yields [30]. Recent research by Boraei et al. has shown a simple and sustainable approach to the creation of tatraazafluoranthenones by using β-ketoesters such as ethyl acetoacetate and ethyl benzoylacetate with ninhydrin in green solvents such as water [31–33].

In this study, we successfully isolated three pivotal intermediates, which unequivocally contribute to the validation of the reaction mechanism leading to the final product formation. Single-crystal diffraction analysis and chemical insights are also explored.

2. Materials and Methods

2.1. General

"Melting points were determined in open capillaries on a Temp-melt II melting point apparatus and the values are uncorrected. Thin layer chromatography (TLC) was carried out on silica gel 60 F_{254} Aluminum plates (E. Merck, layer thickness 0.2 mm). The spots detected by UV lamp. The ^{1}H, ^{13}C-NMR spectra recorded on Bruker 400 MHz-NMR spectrometer operating at 400 and 101 MHz respectively using DMSO-d_6 and $CDCl_3$ as solvent, at the Microanalytical units of Suhag and Mansora University, Egypt. Elemental analysis performed on a Flash EA-1112 instrument".

2.2. Procedures

The synthesis of 4-Methyl/phenyl-1,2,5,6-tetraazafluoranthen-3(2*H*)-ones **4** and **7** from nihydrin is described in [32,33].

2.3. Synthesis of the Intermediates Indeno[1,2-c]Pyridazine-4-Carboxylate **8** *and* **9**

Separately to ethyl 3a,8b-dihydroxy-2-methyl-4-oxo-3a,8b-dihydro-4*H*-indeno[1,2-*b*]furan-3-carboxylate **3** (10 mmol, 2.9 g)/ethyl 2-(2-hydroxy-1,3-dioxo-2,3-dihydro-1*H*-inden-2-yl)-3-oxo-3-phenylpropanoate **6** (10 mmol, 3.5 g) in MeOH (5 mL), NH_2NH_2,H_2O (0.3 mL) was added drop-wise, and the mixture was continuously stirred at room temperature for one hour. The solid product was filtered off and collected and then purified via crystallization from MeOH (**8**) and *n*-hexane (**9**).

2.4. Ethyl 3-Methyl-5-Oxo-5H-Indeno[1,2-c]Pyridazine-4-Carboxylate **8**

Yield 59%, 1.58 g, m.p. 125–126 °C. ^{1}H NMR (400 MHz, DMSO-d_6) δ 8.05 (d, J = 7.5 Hz, 1H), 7.81 (dd, J = 13.3, 7.1 Hz, 2H), 7.64 (t, J = 7.3 Hz, 1H), 4.49 (q, J = 7.1 Hz, 2H), 1.39 (t,

J = 7.1 Hz, 3H); ^{13}C NMR (101 MHz, DMSO) δ 188.72, 163.97, 160.33, 156.50, 141.79, 137.14, 134.64, 132.94, 125.84, 125.75, 125.46, 122.23, 63.01, 20.14, 14.29; elemental analysis calc. for [$C_{15}H_{12}N_2O_3$]: C, 67.16; H, 4.51; N, 10.44; found: C, 67.27; H, 4.55; N, 10.35.

2.5. Ethyl 5-Oxo-3-Phenyl-5H-Indeno[1,2-c]Pyridazine-4-Carboxylate **10**

Yield 53%, 1.74 g, m.p. 95–96 °C. ^{1}H NMR (400 MHz, $CDCl_3$) δ 8.25 (d, *J* = 7.5 Hz, 1H), 7.88 (d, *J* = 7.5 Hz, 1H), 7.82–7.76 (m, 3H), 7.61 (td, *J* = 7.5, 0.8 Hz, 1H), 7.55–7.53 (m, 3H), 4.45 (q, *J* = 7.2 Hz, 2H), 1.31 (t, *J* = 7.2 Hz, 3H); ^{13}C NMR (101 MHz, $CDCl_3$) δ 188.33, 163.88, 160.29, 157.89, 141.46, 136.69, 135.39, 134.61, 132.60, 130.34, 128.83, 128.64, 126.52, 126.47, 125.41, 122.79, 63.00, 13.81; elemental analysis calc. for [$C_{20}H_{14}N_2O_3$]: C, 72.72; H, 4.27; N, 8.48; found: C, 72.88; H, 4.25; N, 8.40.

2.6. Synthesis of 5-Oxo-3-Phenyl-5H-Indeno[1,2-c]Pyridazine-4-Carbohydrazide **11**

To ethyl 2-(2-hydroxy-1,3-dioxo-2,3-dihydro-1*H*-inden-2-yl)-3-oxo-3-phenylpropanoate **6** (10.0 mmol, 3.5 g) in MeOH (5 mL), NH_2NH_2, H_2O (1.0 mL) was added drop-wise, and the mixture was continuously stirred at room temperature overnight. The solid product was filtered off and collected and then purified via crystallization from DMF/MeOH.

Yield 46%, 1.44 g, m.p. >300 °C. ^{1}H NMR (400 MHz, DMSO-d_6) δ ^{1}H NMR (400 MHz, DMSO-d_6) δ 9.80 (s, 1H), 8.19 (d, *J* = 7.4 Hz, 1H), 7.93–7.86 (m, 2H), 7.81–7.79 (m, 2H), 7.72 (t, *J* = 7.5 Hz, 1H),7.60–7.50 (m, 3H), 4.62 (br, 2H); ^{13}C NMR (101 MHz, DMSO) δ 189.03, 161.99, 160.49, 158.81, 141.33, 137.28, 136.29, 134.88, 133.22, 130.64, 130.29, 129.07, 129.04, 129.00, 128.15, 127.16, 125.54, 122.40; elemental analysis calc. for [$C_{18}H_{12}N_4O_2$]: C, 68.35; H, 3.82; N, 17.71; found: C, 68.39; H, 3.91; N, 17.73.

2.7. Synthesis of 3-Phenyl-5H-Indeno[1,2-c]Pyridazine-4-Carbohydrazide **12**

To ethyl 2-(2-hydroxy-1,3-dioxo-2,3-dihydro-1*H*-inden-2-yl)-3-oxo-3-phenylpropanoate **6** (10.0 mmol, 3.5 g) in MeOH (10 mL), NH_2NH_2, H_2O (4.0 mL) was added dropwise, and the mixture was refluxed for 30 min. The formed precipitate was filtered and identified as **7** with 30% yield, 0.89 g. After recrystallization from DMF, the filtrate was left on reflux for a further 3 hrs, dried, washed and recrystallized from EtOH to give **12**.

Yield 49%, 1.54 g, m.p. 241–242 °C. ^{1}H NMR (400 MHz, DMSO-d_6) δ 9.89 (s, 1H), 8.26 (d, *J* = 6.5 Hz, 1H), 7.80–7.78 (m, 3H), 7.63–7.61 (m, 2H), 7.54–7.53 (m, 3H), 4.63 (s, 2H), 4.13 (s, 2H); ^{13}C NMR (101 MHz, DMSO-d_6) δ 164.44, 161.77, 154.87, 144.04, 139.57, 137.30, 137.18, 131.23, 130.93, 129.63, 129.17, 128.95, 128.46, 126.55, 121.70, 34.07; elemental analysis calc. for [$C_{18}H_{14}N_4O$]: C, 71.51; H, 4.67; N, 18.53; found: C, 71.63; H, 4.71; N, 18.50.

2.8. X-ray Structure Determination

The crystal structures of **8**, **10**, **11** and **12** were determined according to the method described in the Supplementary Data [34–37]. The crystal data are presented in Table 1. Crystal Explorer 17.5 software was used for Hirshfeld calculations [38].

Table 1. Crystal data.

	8	**10**	**11**	**12**
CCDC	2297471	2297472	2297470	2299618
Empirical formula	$C_{15}H_{12}N_2O_3$	$C_{20}H_{14}N_2O_3$	$C_{18}H_{12}N_4O_2$	$C_{18}H_{14}N_4O$
fw	268.27	330.33	316.32	302.33
Temp (K)	120(2)	120(2)	120(2)	120(2)
λ(Å)	1.54184	1.54184	1.54184	1.54184
Cryst syst	*Monoclinic*	*Monoclinic*	*Monoclinic*	*Orthorhombic*
Space group	$P2_1/c$	$P2_1/n$	$P2_1/c$	$P2_12_12_1$
a (Å)	15.3400(4)	16.89752(13)	14.9862(2)	5.04710(10)
b (Å)	5.02920(10)	5.76627(4)	4.86410(10)	12.5114(3)
c (Å)	16.7042(4)	17.97633(13)	20.3991(3)	22.2915(5)

Table 1. *Cont.*

	8	10	11	12
β (deg)	100.545(2)	113.9469(9)	101.697(2)	90
V (Å^3)	1266.93(5)	1600.77(2)	1456.10(4)	1407.63(5)
Z	4	4	4	4
ρ_{calc} (Mg/m^3)	1.406	1.371	1.443	1.427
μ(Mo Kα) (mm^{-1})	0.825	0.766	0.804	0.745
No. of reflns.	14014	35632	17874	10944
Unique reflns.	2666	3465	3050	2929
Completeness to θ = 67.684°	100%	100%	100%	100%
GOOF (F^2)	1.054	1.053	1.047	1.046
R_{int}	0.0361	0.0237	0.0295	0.0462
R_1 [a] ($I \geq 2\sigma$)	0.0346	0.0358	0.0397	0.0332
wR_2 [b] ($I \geq 2\sigma$)	0.0863	0.0927	0.1041	0.0768

[a] $R_1 = \Sigma||F_o| - |F_c||/\Sigma|F_o|$. [b] $wR_2 = \{\Sigma[w(F_o^2 - F_c^2)^2]/\Sigma[w(F_o^2)^2]\}^{1/2}$.

3. Results and Discussion

Previously, we reported a simple efficient method for the synthesis of 4-methyl/phenyl-1,2,5,6-tetraazafluoranthen-3(2*H*)-one **4** and **7** from ninhydrin through a reaction first with ethyl acetoacetate or ethyl benzoylacetate and then a reaction of the resultant esters with hydrazine hydrate [32,33] (Scheme 1).

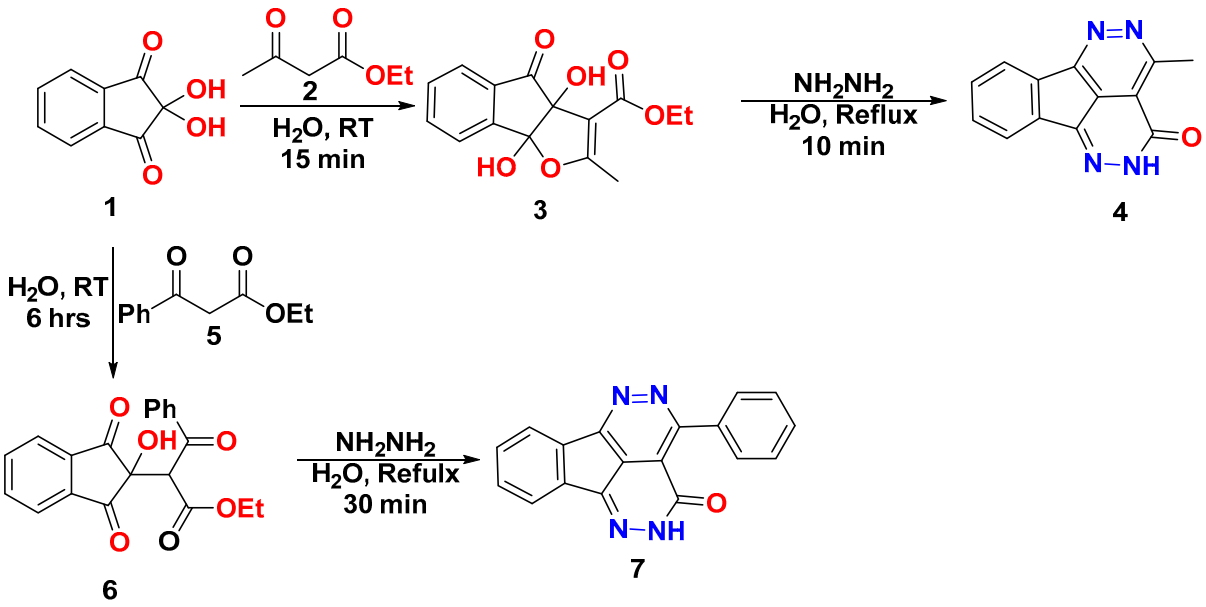

Scheme 1. Synthesis of tetraazafluoranthen-3(2*H*)-ones **4** and **7** [32,33].

According to the reported mechanism for tetraazafluoranthen-3(2*H*)-one **4** formation that was suggested theoretically and initially proposed, ethyl acetoacetate was condensed with ninhydrin to afford ethyl indeno[1,2-*b*]furan-3-carboxylate **3**. Subsequently, the carbonyl was attached via two moles of hydrazine, the furan ring of which was cleaved, and four molecules of water, and ethanol was kicked out. During this process, recyclization occurred to form tetraazafluoranthen-3-one [32] (Scheme 2). However, the real steps involved in the mechanism allowing the final products to be obtained in that reaction are unclear.

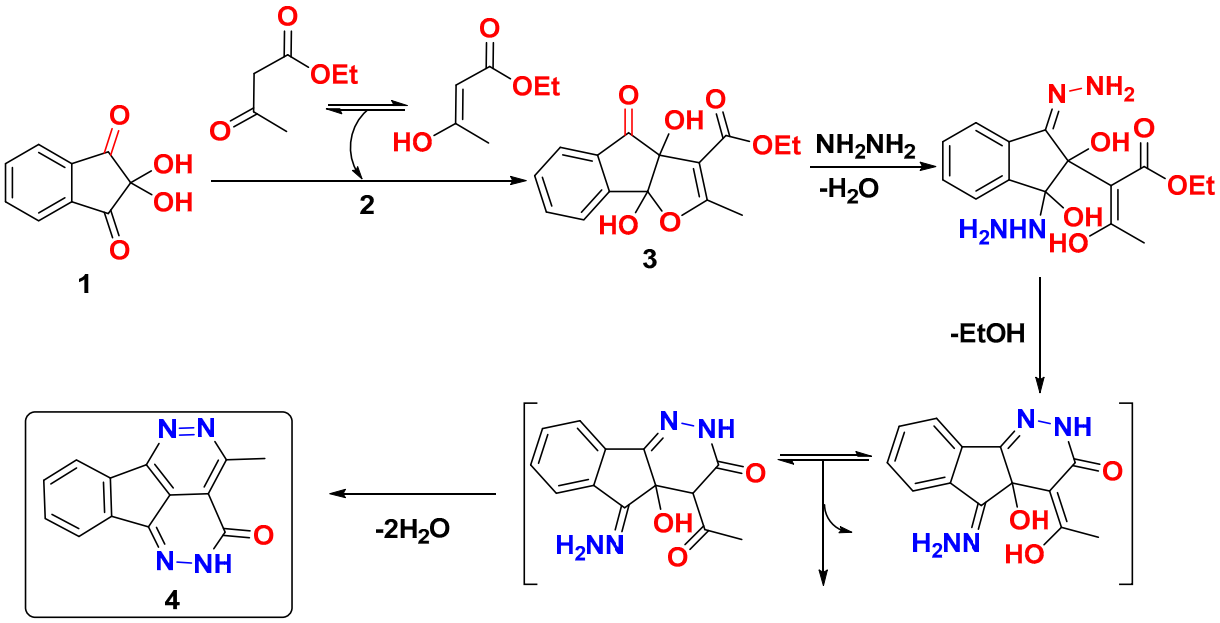

Scheme 2. Proposed mechanism of the formation of tetraazafluoranthen-3-one **4** [32].

Herein, the important intermediates in this reaction are identified. Ethyl 3-methyl-5-oxo-5*H*-indeno[1,2-*c*]pyridazine-4-carboxylate **8** was obtained from the reaction of ethyl 3a,8b-dihydroxy-2-methyl-4-oxo-3a,8b-dihydro-4*H*-indeno[1,2-*b*]furan-3-carboxylate **3** with hydrazine hydrate after stirring for only one hour (Scheme 3). The isolation of this intermediate proves that the first hydrazine molecule attacked the keto group and furan ring to form 3-methyl/phenyl-5-oxo-5*H*-indeno[1,2-c]pyridazine-4-carboxylate **8**, whereas the second hydrazine molecule attacked the ester group and then cyclized to afford tetraazafluoranthen-3-one **4**. Trials for the separation of hydrazide **9** via either reducing the duration of the reaction or reducing the amount of hydrazine failed. It seems that as long as hydrazide **9** is formed, it is converted to **4**. The structures of **8** were confirmed based on NMR, in which the ethyl ester protons were found at 1.39 ppm for CH_3 and 4.49 ppm for OCH_2, and the respective ethyl carbons were detected at 14.29 ppm (CH_3) and 63.01 ppm (OCH_2). The carbonyl carbon of the ketone group was observed at 188.72 ppm, while the carbonyl carbon of the ester was found at 163.97 ppm.

In a further study to identify the intermediates included through tetraazafluoranthen-3-one's formation, ethyl 2-(2-hydroxy-1,3-dioxo-2,3-dihydro-1*H*-inden-2-yl)-3-oxo-3-phenylpropanoate **6** was reacted with hydrazine hydrate through stirring at room temperature for one hour to give ethyl 5-oxo-3-phenyl-5*H*-indeno[1,2-*c*]pyridazine-4-carboxylate **10**, which reacted with another hydrazine molecule to give the hydrazide 5-oxo-3-phenyl-5*H*-indeno[1,2-c]pyridazine-4-carbohydrazide **11**. Separation of the intermediate hydrazide **11** confirmed that the second hydrazine molecule attacked the ester group and then the carbonyl group of the indene moiety to form the cyclized tetraazafluoranthen-3-one **7**; furthermore, in the presence of hydrazine and ethanol, the carbonyl of the indenone moiety was subjected to a Wolff–Kishner-like reduction to give **12**. This reduction reflects the role of phenyl group in the stability of hydrazide **11** over hydrazide **9**, which has a methyl group (Scheme 4). The NMR of ester **10** displayed ethyl protons of the ester group at 1.31 ppm (CH_3) and 4.45 ppm (OCH_2), whereas the respective carbons appeared at 13.81 ppm and 63.00 ppm. The carbonyl carbons of the ester and ketone groups appeared at 163.88 and 188.33 ppm, respectively. The NMR of hydrazide **11** displayed the hydrzino group protons ($NHNH_2$), which appeared at 9.80 ppm for NH and 4.62 ppm for NH_2. The carbonyl carbon of the ketone group was observed at 189.03 ppm, while the carbonyl carbon of the hydrazide group was found at 161.99 ppm. Hydrazide **12** displayed the $-NHNH_2$ group protons at 9.89 ppm and 4.63 ppm, respectively. The methylene protons formed by the

reduction were found at 4.13 ppm. ^{13}C NMR displayed the carbonyl carbon of the ester group at 164.44 ppm and the methylene carbon resulted from the reduction at 34.07 ppm.

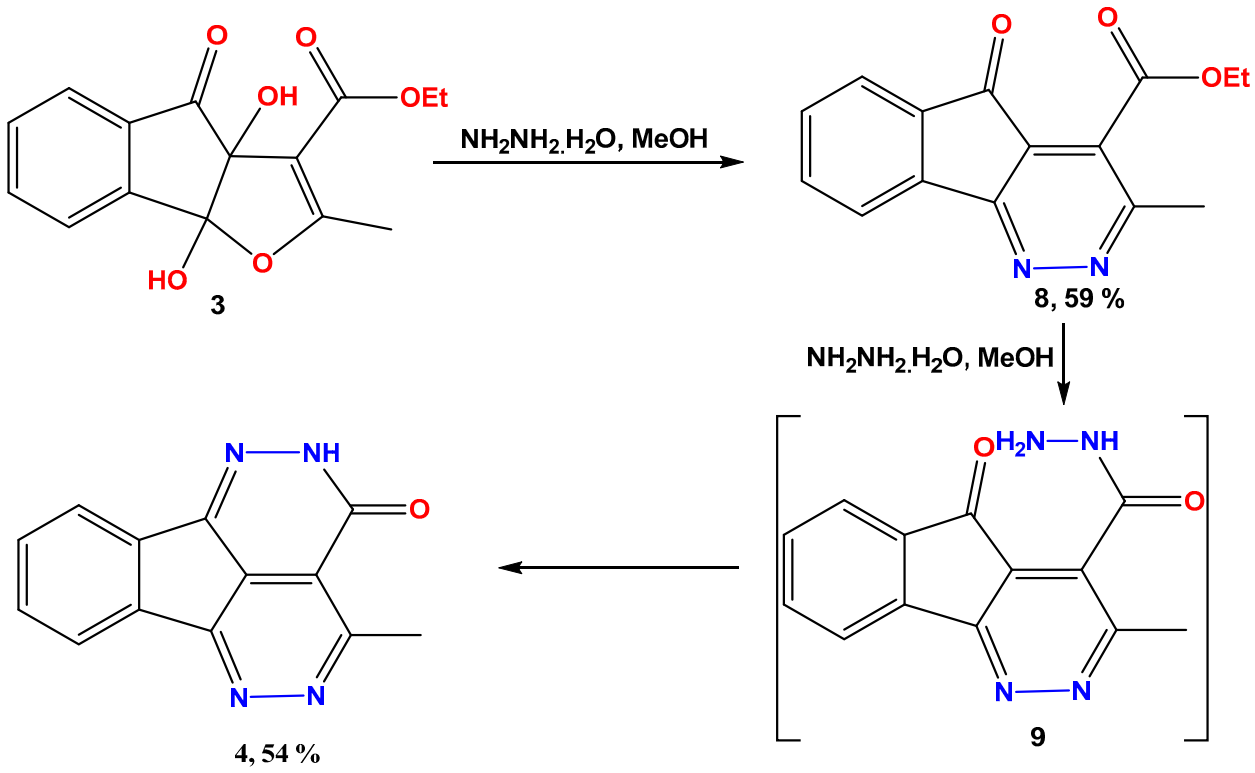

Scheme 3. Synthesis of tetraazafluoranthen-3-one **4**: one separated intermediate, **8**.

The X-ray structure of **11** is shown in Figure 1. Relevant bond distances and angles are given in Table S1 (Supplementary Data). **11** crystallized in the monoclinic crystal system and centrosymmetric $P2_1/c$ space group, where a = 14.9862(2) Å, b = 4.86410(10) Å, c = 20.3991(3) and β = 101.697(2)°. One molecule of **11** is the asymmetric formula. The structure of the fused ring system comprised three rings, A, B and C, which were not perfectly coplanar. The mean planes of rings B and C formed angles of 2.74° and 4.24° with respect to the plane of ring A. The phenyl ring D and the fused ring system C were twisted around one another at a 39.76° angle.

The crystal structure of **11** is controlled by the N3-H3...O2, N4-H4A...O1 and N4-H4B...N4 contacts shown in Figure 2A. The respective H. . .A distances are 1.93(2), 2.52(2) and 2.16(2) Å, while the D. . .A distances are 2.8614(16), 3.0425(16) and 3.1152(16) Å, respectively. An illustration of the hydrogen bonding scheme is shown in Figure 2B. Additionally, one weak C7-H7. . .N1 interaction with a C7. . .N1 distance of 3.3167(18) Å was removed from the packing scheme for more clarity.

In Figure 3, the X-ray structure of **8** is shown. As indicated by the crystallographic parameters, **8** is also crystallized in the same crystallographic system and with the same space group as **11** (Table 1). In the case of compound **8**, the values a = 15.3400(4) Å, b = 5.02920(10) Å, c = 16.7042(4) Å and β =100.545(2)° are different. The asymmetric unit contains one molecule of **8**, while z = 4. In this case, the three rings, A, B and C, are also not fully coplanar with each other. The angles between rings B and C with the central ring A are 2.17° and 1.15°, respectively. As a result, the fused ring system is more planar than that found for **11**.

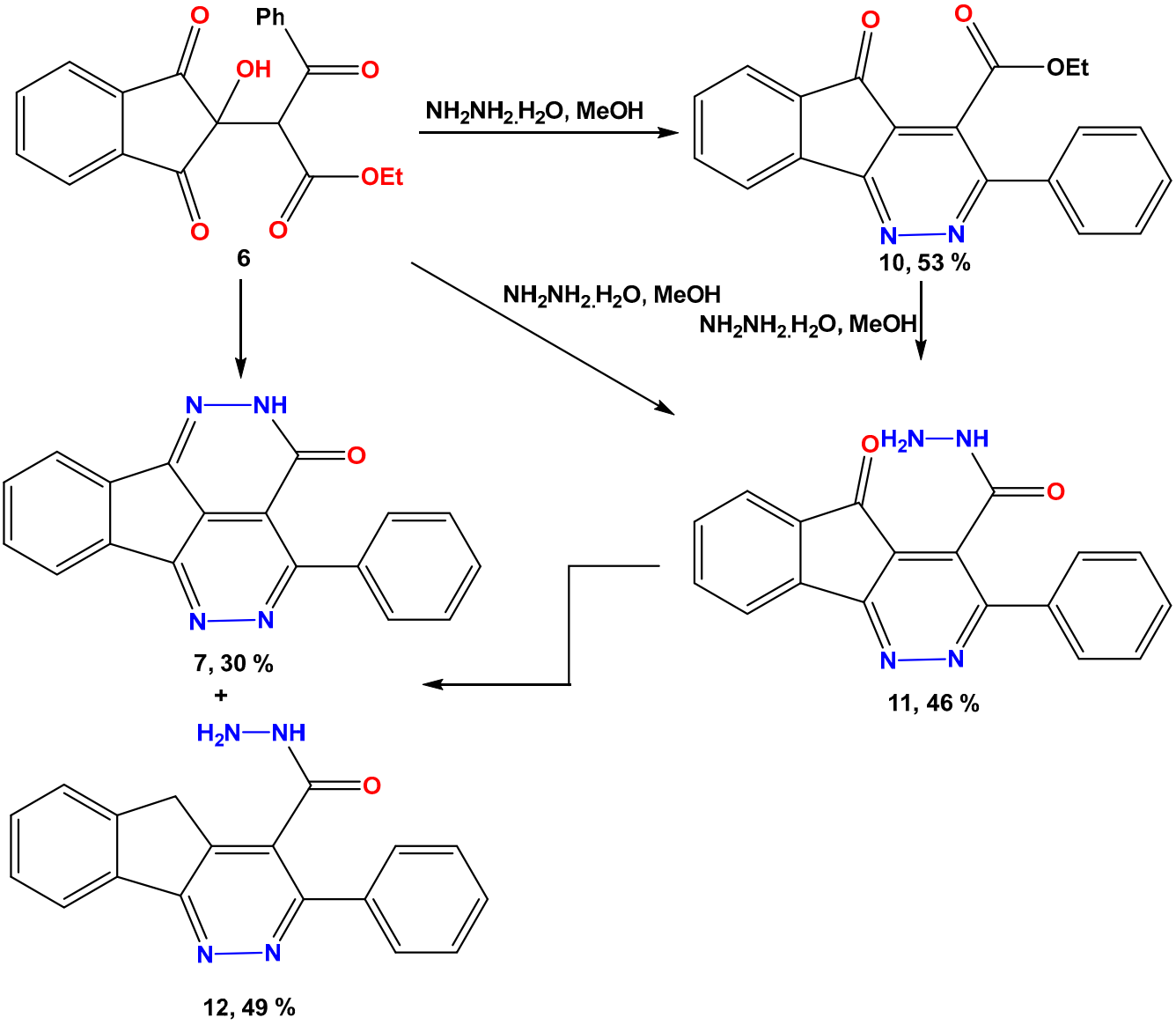

Scheme 4. Synthesis of tetraazafluoranthen-3-one **7**: two separated intermediates, **10** and **11**.

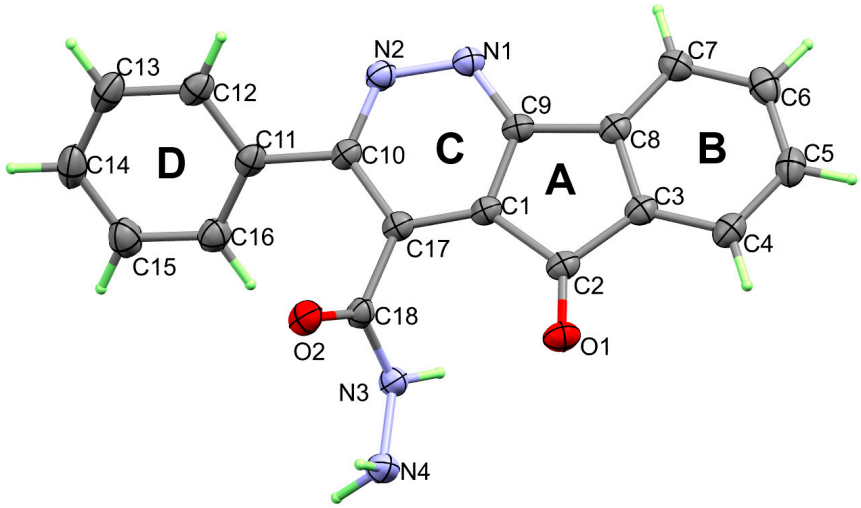

Figure 1. X-ray structure of **11**.

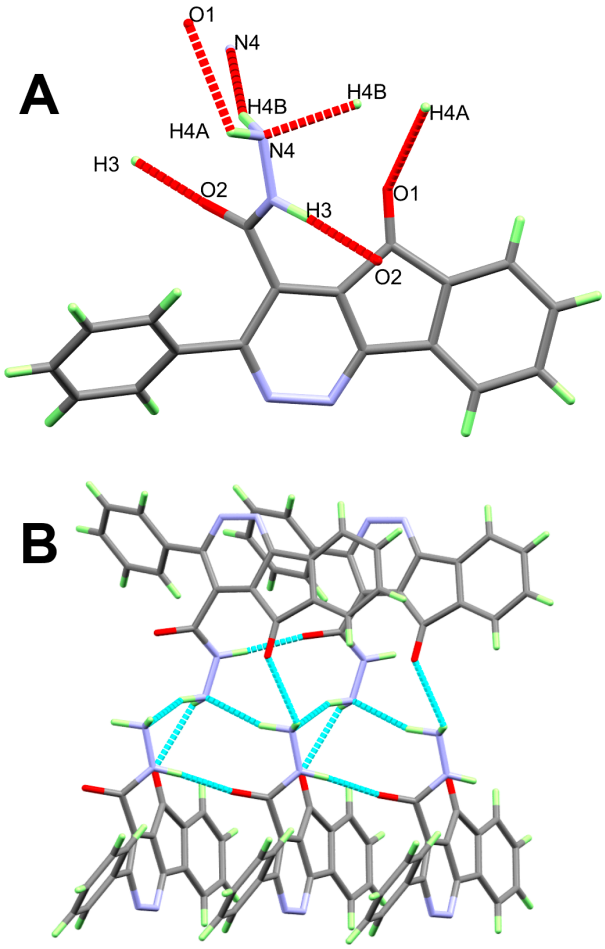

Figure 2. The O. . .H/N. . .H interactions (**A**) and packing view (**B**) for **11**. For the H-bond details, see Table 2.

Table 2. Hydrogen bonds for **11**, **8**, **10** and **12** (Å and °) [a].

D-H...A	d(D-H)	d(H...A)	d(D...A)	<(DHA)	Symm. Code
11					
N3-H3...O2#1	0.94(2)	1.93(2)	2.8614(16)	175.0(19)	x, y + 1, z
N4-H4A...O1#2	0.98(2)	2.52(2)	3.0425(16)	113.3(15)	−x + 1, y − 1/2, −z + 3/2
N4-H4B...N4#2	1.01(2)	2.16(2)	3.1152(16)	157.7(19)	−x + 1, y − 1/2, −z + 3/2
8					
C13. . .H13C. . .O1	0.98	2.6368	3.331(2)	128	1 − x, −1/2 + y,1.5 − z
10					
C4-H4...N1	0.95	2.44	3.3764(14)	167	1 − x, −y, 1 − z
C4-H4...N2	0.95	2.6	3.4325(14)	146	1 − x, −y, 1 − z
C14-H14...O1	0.95	2.58	3.3447(15)	137	−1/2 + x, 3/2 − y, −1/2 + z
C19-H19B...O2	0.99	2.44	3.4061(14)	165	x, 1 + y, z
C20-H20C...O1	0.98	2.58	3.3182(19)	132	x, 1 + y, z
12					
N11-H11...O11	0.89(3)	2.06(3)	2.852(3)	147(2)	−1 + x, y, z
N12-H12A...O11	0.89(3)	2.34(3)	3.174(3)	156(2)	−1/2 + x, 3/2 − y, 1 − z
C11-H11B...O11	0.99	2.36	3.317(3)	163	−1 + x, y, z

[a] Donor (D) and acceptor (A).

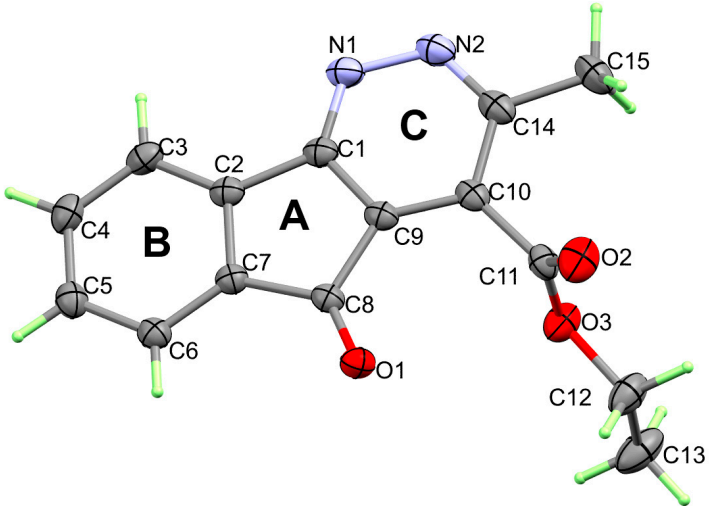

Figure 3. X-ray structure of **8**.

In **8**, the packing is controlled by weak C-H. . .O contacts (Table 2 and Figure 4A). The donor–acceptor distance of the C13. . .H13C. . .O1 interaction is 3.331(2) Å. The packing view for the crystal structure of **8** is shown in Figure 4B.

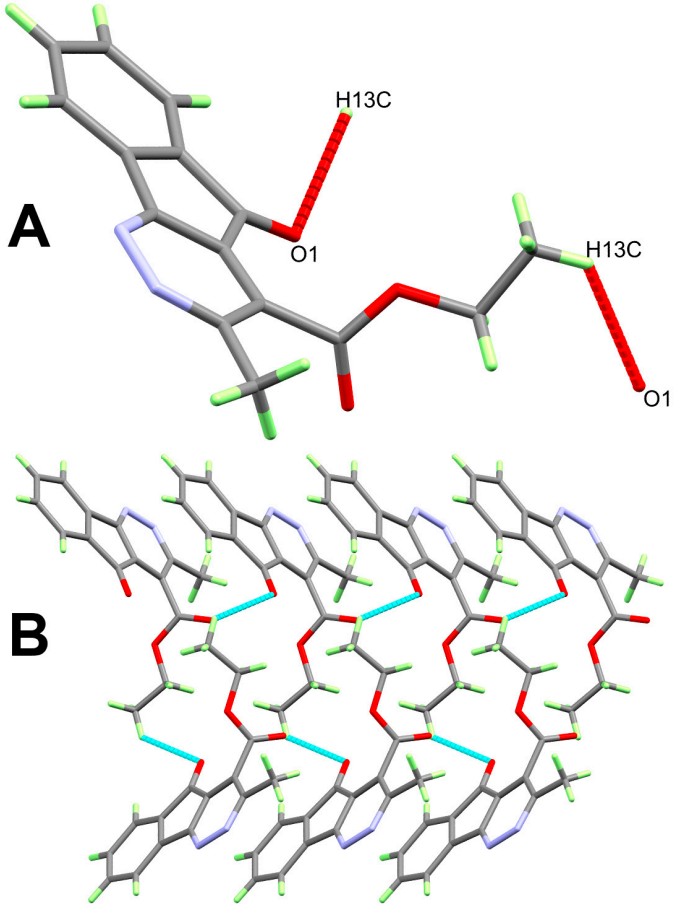

Figure 4. The O. . .H interactions (**A**) and packing view (**B**) for **8**.

In Figure 5, the X-ray structure of **10** is shown. Similar to the other two compounds, compound **10** is also crystallized in the monoclinic crystal system with the lattice parameters a = 16.89752(13), b = 5.76627(4) Å, c = 17.97633(13) Å and β = 113.9469(9)°. The asymmetric unit contains one molecule of **10**. In this case, the three rings, A, B and C, are also not fully

coplanar with each other. The angles between rings B and C with the central ring A are 5.32° and 5.27°, respectively, showing the maximum deviation from planarity in this case. The phenyl ring D and the fused ring C deviate significantly by 43.07°, which is also a larger difference than that found in **11**.

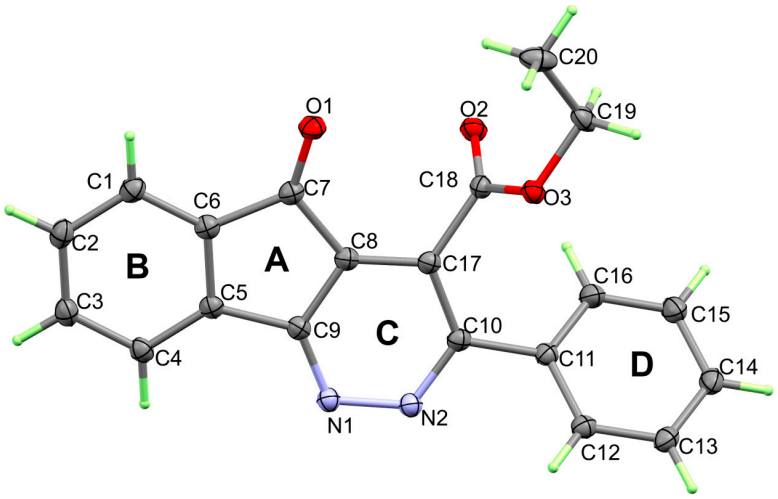

Figure 5. X-ray structure of **10**.

The crystal structure of **10** is controlled by the weak C-H. . .N and C-H. . .O interactions shown in Figure 6. The corresponding hydrogen bond parameters are listed in Table 2. There are three C-H. . .O interactions: C14-H14...O1, C19-H19B...O2 and C20-H20C...O1. The D. . .A distances are 3.3447(15), 3.4061(14) and 3.3182(19) Å, respectively. On the other hand, the two less important C-H. . .N interactions are the C4-H4...N1 and C4-H4...N2 contacts, where the C4. . .N1/N2 distances are 3.3764(14) and 3.4325(14) Å, respectively.

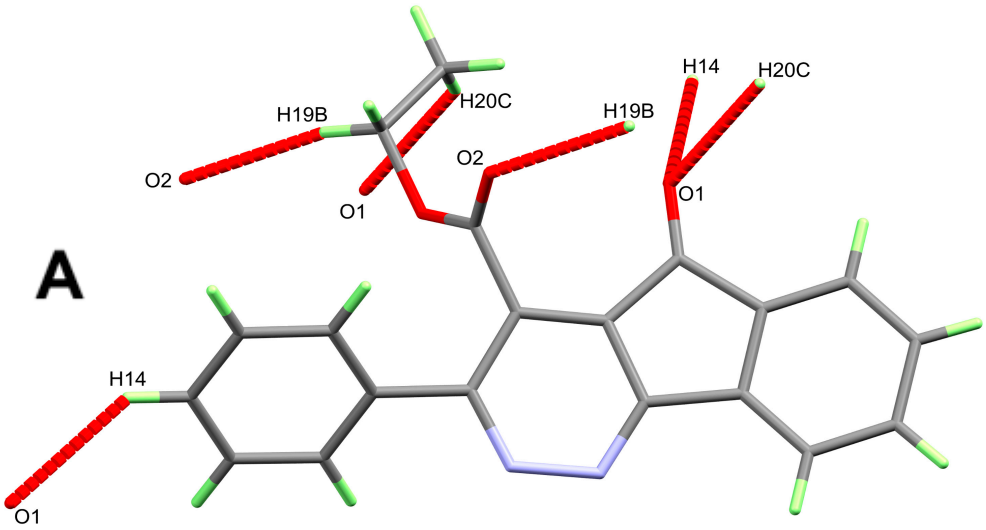

Figure 6. *Cont*.

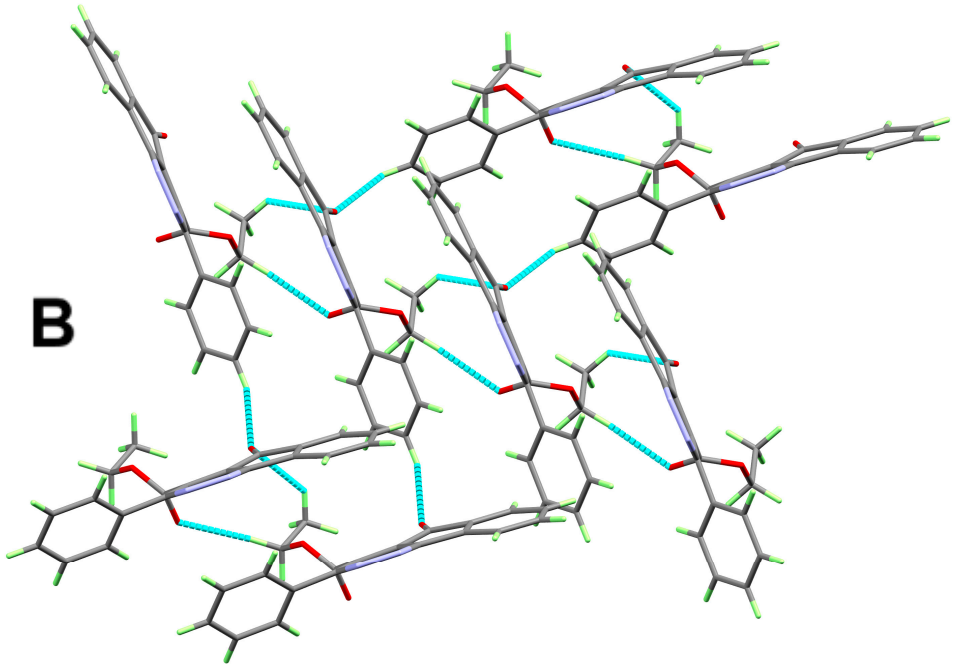

Figure 6. The O. . .H/N. . .H interactions (**A**) and packing structure (**B**) for **10**.

The structure of **12** showing atom numbering is presented in Figure 7. It crystallized in the *orthorhombic* system (a = 5.04710(10) Å, b = 12.5114(3) and c = 22.2915(5) Å) and centrosymmetric $P2_12_12_1$ space group. The crystal density is 1.427 Mg/m^3 and the unit cell volume is 1407.63(5) Å^3. In this compound, the mean planes of rings B and C make angles of 2.42° and 2.31° with respect to the plane of ring A. The phenyl ring D and the fused ring system C showed a twist of 31.26°.

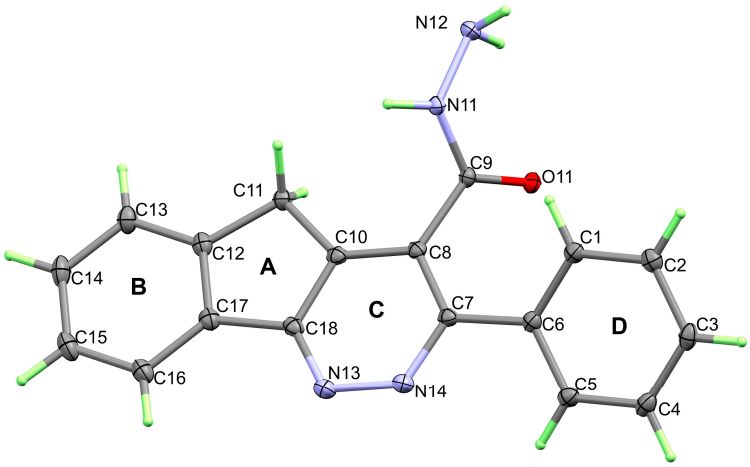

Figure 7. X-ray structure of **12**.

The crystal structure of **12** is stabilized by the intermolecular N12-H12A...O11, and N11-H11...O11 hydrogen bonds are important for the molecular packing of **12**. The H12A...O11 and H11...O11 distances are 2.852(3) and 3.174(3) Å, respectively. Also, the weak C11-H11B...O11 interaction is also important for molecular packing. For this interaction, the C11...O11 distance is 3.317(3) Å (Table 2). An illustration of these intramolecular hydrogen bonding interactions, along with the packing scheme, is shown in Figure 8.

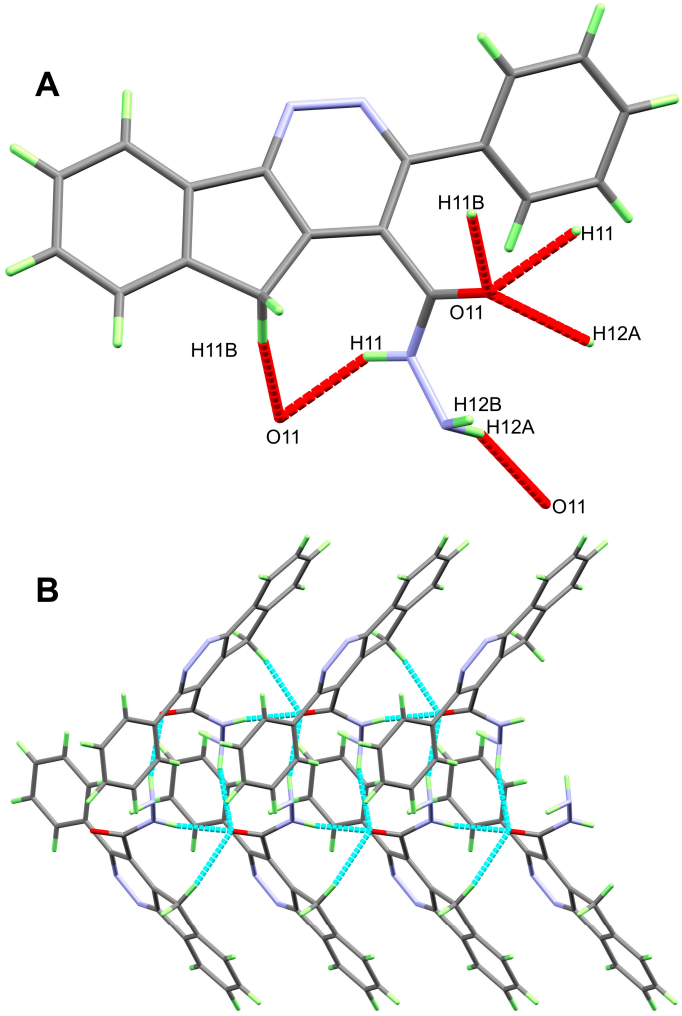

Figure 8. The O. . .H interactions (**A**) and packing view (**B**) for **12**.

Hirshfeld Surface Analysis

The possible contacts in the crystal structure of **11** were analyzed using the d_{norm} Hirshfled map shown in Figure 9. The structure of this crystal is stabilized by short N4. . .H4B, N1. . .H7, N2. . .H7, O1. . .H4A and O2. . .H3 hydrogen bonds. The respective hydrogen-to-acceptor distances are 2.158, 2.244, 2.61, 2.509 and 1.855 Å. Also, C13. . .H4 (2.655 Å) and C6. . .H5 (2.717 Å) interactions were detected and found to be important for the crystal structure stability (Table 3). Additionally, the packing of molecules was found to be controlled by other short, non-covalent interactions such as C1. . .O2 (3.050 Å) and C2. . .O2 (2.929 Å). All these short contacts appeared in the d_{norm} map as red spots, indicating short contacts compared to the vdWs radii sum of the interacting atoms.

Table 3. Short contacts in **11**.

Contact	Distance	Contact	Distance
C1. . .O2	3.050	O1. . .H4A	2.509
C2. . .O2	2.929	O2. . .H3	1.855
N4. . .H4B	2.158	C13. . .H4	2.655
N1. . .H7	2.244	C6. . .H5	2.717
N2. . .H7	2.610		

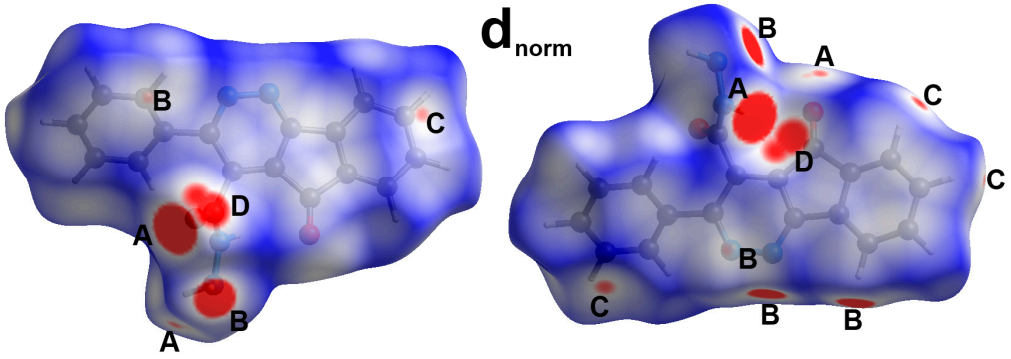

Figure 9. The d_{norm} Hirshfeld surface of **11**: (A) O. . .H, (B) N. . .H, (C) C. . .H, (D) C. . .O.

The fingerprint plot is not only important for identifying and decomposing all intermolecular contacts but also for predicting their importance in the molecular packing. The H. . .H (37.4%), C. . .H (16.7%), N. . .H (15.3%), O. . .H (14.2%) and C. . .C (10.4%) contacts had the largest contribution (Figure 10). Other less common contacts, such as C. . .O (3.5%), C. . .N (1.6%), O. . .O (0.5%), N. . .N (0.2%) and N. . .O (0.2%), were also detected. Only the O. . .H, N. . .H, C. . .H and C. . .O interactions appeared as sharp spikes in the decomposed fingerprint (FP) plots, which is considered as further evidence for their importance in molecular packing (Figure S9; Supplementary Data).

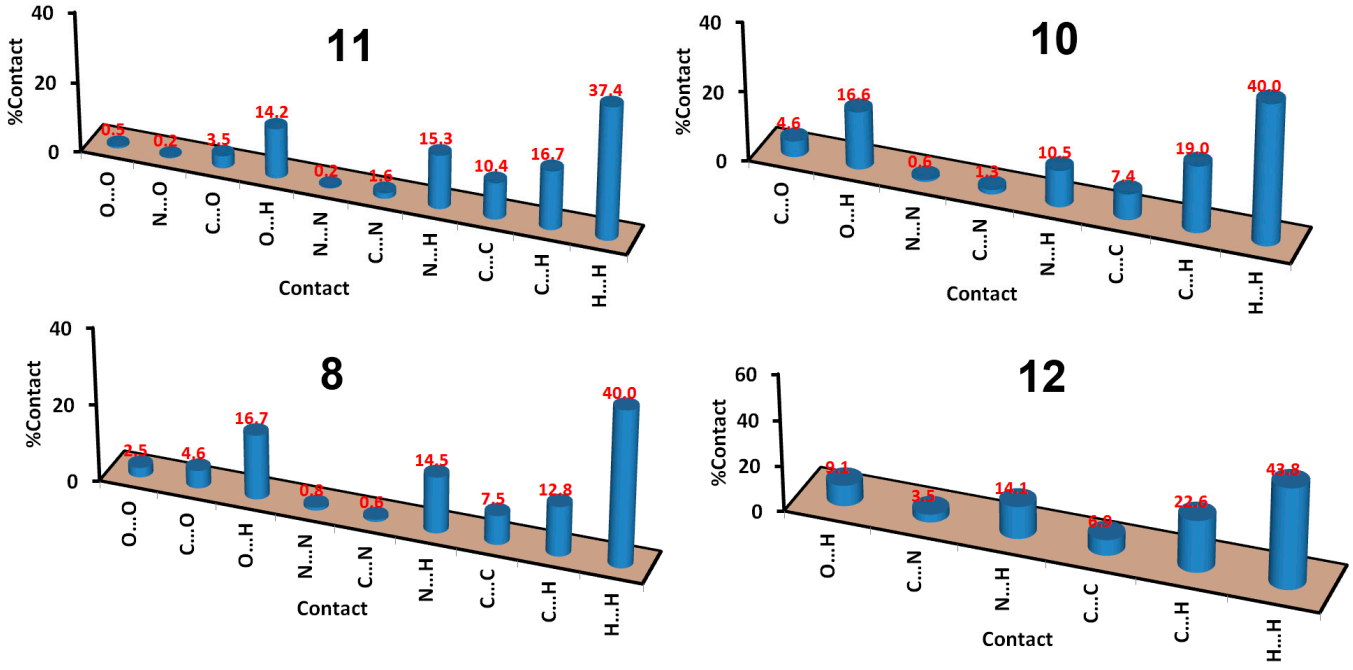

Figure 10. All contacts in the studied compounds.

In the case of the crystal structure of **8**, the d_{norm} Hirshfeld map shown in Figure 11 indicates the importance of the O1. . .H13C (2.575 Å), C5. . .H4 (2.747 Å), C4. . .H5 (2.762 Å), H3. . .H3 (1.911 Å), C8. . .O2 (2.853Å) and C9. . .O2 (3.200 Å) interactions. Also, these interactions have the characteristic features of short significant contacts in both d_{norm} maps and fingerprint plots (Figure S10; Supplementary Data). It is clear that there were no important N. . .H contacts detected in this case. Also, the percentages of all possible contacts in **8** were obtained from the FP plots, and the results are presented graphically in Figure 10. The H. . .H (40.0%), O. . .H (16.7%), N. . .H (14.5%) and C. . .H (12.8%) contacts are the most common in this crystal structure. Other minor contacts, such as C. . .C (7.5%), C. . .O (4.6%), O. . .O (2.5%), N. . .N (0.8%) and C. . .N (0.6%), were also observed.

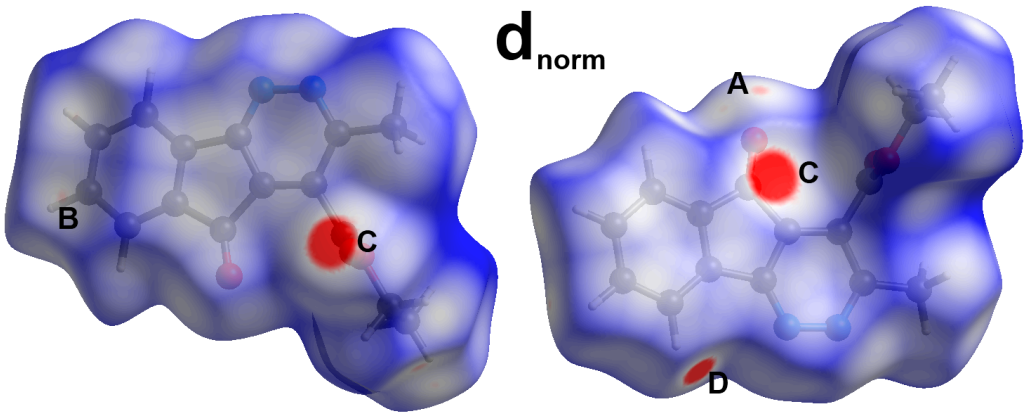

Figure 11. The d_{norm} maps of **8**; (A) O. . .H, (B) C. . .H, (C) C. . .O, (D) H. . .H.

For **10**, the d_{norm} Hirshfeld surface is shown in Figure 12. There are four types of strong intermolecular interactions: O...H, N...H, C...H and C...O contacts. The O1. . .H14 (2.488 Å), O2. . .H19B (2.349 Å), O1. . .H20C (2.516 Å), N2. . .H4 (2.493 Å), N1. . .H4 (2.315 Å), C13. . .H1 (2.76 Å) and C7. . .O3 (3.115 Å) contacts are non-covalent interactions with distances significantly shorter than the vdWs radii sum of the interacting atoms. Hence, these non-covalent interactions have great significance in the molecular packing of **10**. Also, these interactions have the characteristic spikes and wings of short, significant contacts (Figure S11; Supplementary Data). In addition, the percentages of all possible contacts in **10** are presented in Figure 10. The H. . .H (40.0%), O. . .H (16.6%), N. . .H (10.5%) and C. . .H (19.0%) contacts are the most common in this crystal structure. Other minor contacts, such as C. . .C (7.4%), C. . .O (4.6%), N. . .N (0.6%) and C. . .N (1.3%), were also observed.

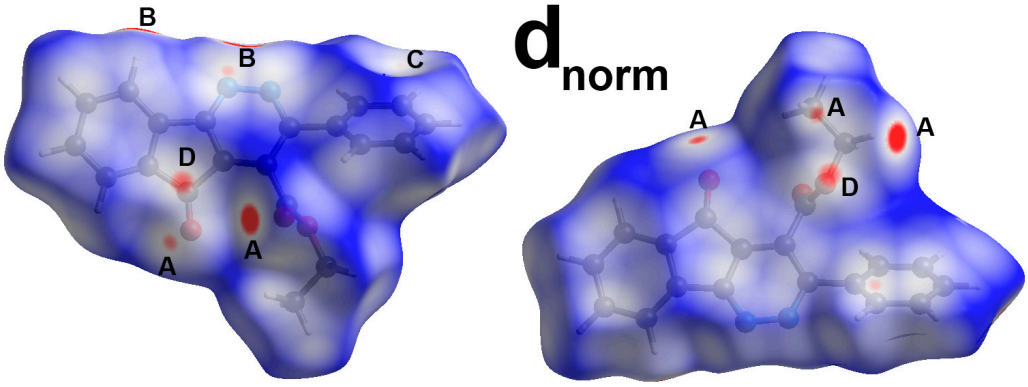

Figure 12. The d_{norm} Hirshfeld surfaces of **10**: (A) O. . .H, (B) N. . .H, (C) C. . .O, (D) C. . .H.

For **12**, the supramolecular structure is controlled by a number of non-covalent interactions, which are the O...H, N...H, C...H, C...C, C...N and H...H contacts. Only the O...H, N...H, C...H and C...C contacts appeared as red spots in the d_{norm} map and are considered important for the molecular packing of compound **12** (Figure 13). The red spots in the d_{norm} map were found to correspond to the O11. . .H12A (2.231 Å), O11. . .H11 (1.965 Å), O11. . .H11B (2.268 Å), C3. . .H4 (2.619 Å), N13. . .H11A (2.461 Å) and C4. . .C7 (3.275 Å) contacts. Also, these interactions have the characteristic spikes and wings of short, significant contacts (Figure S12; Supplementary Data). In addition, the percentages of all possible contacts in **12** are presented in Figure 10. The H. . .H (43.8%), C. . .H (22.6%), N. . .H (14.1%) and O. . .H (9.1%) contacts are the most common, while C. . .C (6.9%) and C. . .C (3.6%) are minor contacts.

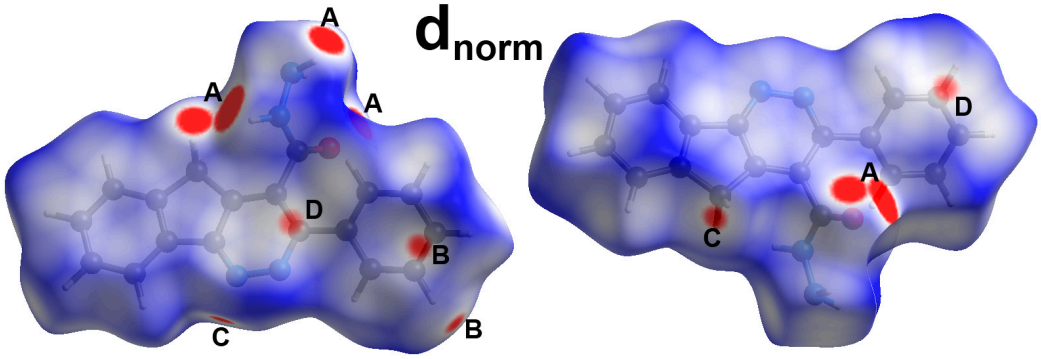

Figure 13. The d_{norm} Hirshfeld surfaces of **12**: (A) O. . .H, (B) C. . .H, (C) N. . .H, (D) C. . .C.

The curvedness and shape index maps presented in Figure S13 (Supplementary Data), which show the characteristic features of π-π interactions. In the curvedness map, there is a green flat area, while in the shape index map, there are red/blue triangles; this provides significant evidence of π-π interactions. The %C. . .C interactions were 10.4, 7.5, 7.4 and 6.9% in compounds **11**, **8**, **10** and **12**, respectively. Generally, the C. . .C contacts had slightly longer distances and twice the vdWs radii sum of carbon for all the studied systems, revealing weak π-π stacking interactions. The most important π-π stacking interactions for the studied systems, including the shortest C. . .C/C. . .N contacts and their interaction distances in Å, are shown in Figure S14 (Supplementary Data).

4. Conclusions

We concluded that the two most important intermediates in the hydrazinolysis–cyclization process of tetraazafluoranthen-3(2*H*)-one synthesis were isolated and characterized. This fact unambiguously proves that the reaction includes the two hydrazinolysis–cyclization reactions: firstly, condensation of hydrazine with two ketone groups, and then the reaction of hydrazine with the ester followed by condensation with the other ketone group. Hydrazide **11** was stable enough to be reduced by hydrazide to give **12**. Structures were confirmed using NMR and single-crystal analysis. X-ray single-crystal structure determinations combined with Hirshfeld topology analysis were used to analyze the structure of the studied compounds. Compounds **11** and **10** have common significant non-covalent interactions, which are the O. . .H, N. . .H, C. . .H and C. . .O contacts, while the supramolecular structure of compound **8** is controlled by O. . .H, C. . .H, C. . .O and H. . .H contacts, where no important N. . .H interactions were detected. The percentage of the O. . .H contacts is the highest in the case of **8** (16.7%) and **10** (16.6%). The C. . .H contacts contributed to 16.7, 12.8 and 19.0% of all non-covalent interactions occurring in **11**, **8** and **10,** respectively, while the %C. . .O interactions accounted for 3.5, 4.6 and 4.6%, respectively. Both **11** and **10** showed important N. . .H interactions, whose percentages were 15.3 and 10.5%, respectively. The N. . .H contacts were less important in the case of **8**, while the H. . .H contacts were found to have great significance. For **12**, the O...H, N...H, C...H and C...C contacts were the most important. Their percentages were 9.1, 14.1, 22.6 and 6.9%, respectively. All compounds showed weak π-π stacking interactions.

Supplementary Materials: The following supporting information can be downloaded at: https://www.mdpi.com/article/10.3390/cryst13111537/s1. Figure S1. 1H NMR of **8**; Figure S2. 13C NMR of **8**; Figure S3. 1H NMR of **10**; Figure S4. 13C NMR of **10**; Figure S5. 1H NMR of **11**; Figure S6. 13C NMR of **11**; Figure S7. 1H NMR of **12**; Figure S8. 13C NMR of **12**; Figures S9–S12: Fingerprint plots for the short interactions in **11**, **8**, **10** and **12**; Figure S13. Shape index and curvedness maps for the studied systems; Figure S14. The most important π-π stacking C. . .C/C. . .N contacts and their interaction distances in Å for the studied systems; X-ray structure determination; Table S1. Bond lengths (Å) and angles (°) for **11**, **8**, **10** and **12**.

Author Contributions: Conceptualization, E.E.S., A.T.A.B., A.A.M.S. and A.B.; methodology, E.E.S., A.A.M.S. and A.T.A.B.; software, S.M.S. and M.H.; validation, E.E.S., A.T.A.B. and A.B.; formal

analysis, E.E.S. and A.T.A.B.; investigation, A.T.A.B.; resources, A.T.A.B. and A.B.; data curation, M.S.; writing—original draft preparation, A.T.A.B.; writing—review and editing, E.E.S., A.T.A.B., A.B., S.M.S., M.H. and A.A.M.S.; visualization, A.T.A.B. and A.B.; supervision, A.T.A.B.; project administration, A.B.; funding acquisition, M.S. All authors have read and agreed to the published version of the manuscript.

Funding: The authors would like to extend their sincere appreciation to the Researchers Supporting Project (RSP2023R64), King Saud University, Riyadh, Saudi Arabia.

Data Availability Statement: Not applicable.

Conflicts of Interest: The authors declare no conflict of interest.

References

1. Feng, X.; Pisula, W.; Müllen, K. Large polycyclic aromatic hydrocarbons: Synthesis and discotic organization. *Pure Appl. Chem.* **2009**, *81*, 2203–2224. [CrossRef]
2. Stępień, M.; Gońka, E.; Żyła, M.; Sprutta, N. Heterocyclic nanographenes and other polycyclic heteroaromatic compounds: Synthetic routes, properties, and applications. *Chem. Rev.* **2017**, *117*, 3479–3716. [CrossRef]
3. Albarano, L.; De Rosa, I.; Santaniello, I.; Montuori, M.; Serafini, S.; Toscanesi, M.; Trifuoggi, M.; Lofrano, G.; Guida, M.; Libralato, G. Synergistic, antagonistic, and additive effects of naphthalene, phenanthrene, fluoranthene and benzo (k) fluoranthene on Artemia franciscana nauplii and adult. *Environ. Pollut.* **2023**, *335*, 122286. [CrossRef]
4. Plunkett, K. What about the five-membered ring? Cyclopentafused polycyclic aromatic hydrocarbons as a building block for functional materials. *Synlett* **2013**, *24*, 898–902. [CrossRef]
5. Brauers, G.; Ebel, R.; Edrada, R.; Wray, V.; Berg, A.; Gräfe, U.; Proksch, P. Hortein, a new natural product from the fungus Hortaea werneckii associated with the Sponge Aplysina aerophoba. *J. Nat. Prod.* **2001**, *64*, 651–652. [CrossRef]
6. Xie, S.; Chen, W.; Liu, S.; Zong, H.; Ming, B.; Zhou, G. Facile synthesis and functionalization of fluoranthenes via intramolecular [4+2] annulations between thiophenes and alkynes. *Chin. Chem. Lett.* **2023**, *34*, 107642. [CrossRef]
7. Goel, A.; Sharma, A.; Kathuria, M.; Bhattacharjee, A.; Verma, A.; Mishra, P.R.; Nazir, A.; Mitra, K. New fluoranthene FLUN-550 as a fluorescent probe for selective staining and quantification of intracellular lipid droplets. *Org. Lett.* **2014**, *16*, 756–759. [CrossRef]
8. Du, L.; King, J.B.; Cichewicz, R.H. Chlorinated polyketide obtained from a Daldinia sp. Treated with the epigenetic modifier suberoylanilide hydroxamic Acid. *J. Nat. Prod.* **2014**, *77*, 2454–2458. [CrossRef]
9. Ding, L.; Ying, H.-Z.; Zhou, Y.; Lei, T.; Pei, J. Polycyclic imide derivatives: Synthesis and effective tuning of lowest unoccupied molecular orbital levels through molecular engineering. *Org. Lett.* **2010**, *12*, 5522–5525. [CrossRef]
10. Chiechi, R.C.; Tseng, R.J.; Marchioni, F.; Yang, Y.; Wudl, F. Efficient Blue-Light-Emitting Electroluminescent Devices with a Robust Fluorophore: 7,8,10-Triphenylfluoranthene. *Adv. Mater.* **2006**, *18*, 325–328. [CrossRef]
11. Yan, Q.; Zhou, Y.; Ni, B.-B.; Ma, Y.; Wang, J.; Pei, J.; Cao, Y. Organic semiconducting materials from sulfur-hetero benzo[k]-fluoranthene derivatives: Synthesis, photophysical properties, and thin film fransistor fabrication. *J. Org. Chem.* **2008**, *73*, 5328–5339. [CrossRef] [PubMed]
12. Goel, A.; Kumar, V.; Chaurasia, S.; Rawat, M.; Prasad, R.; Anand, R.S. Synthesis, electrochemical and optical properties of stable yellow fluorescent fluoranthenes. *J. Org. Chem.* **2010**, *75*, 3656–3662. [CrossRef] [PubMed]
13. Wu, H.; Fang, R.; Tao, J.; Wang, D.; Qiao, X.; Yang, X.; Hartl, F.; Li, H. Diacenaphthylene-fused benzo [1, 2-b: 4, 5-b'] dithiophenes: Polycyclic heteroacenes containing full-carbon five-membered aromatic rings. *Chem. Commun.* **2017**, *53*, 751–754. [CrossRef] [PubMed]
14. Rice, J.E.; Cai, Z.W. An intramolecular arene-triflate coupling reaction for the regiospecific synthesis of substituted benzofluoranthenes. *J. Org. Chem.* **1993**, *58*, 1415–1424. [CrossRef]
15. Gu, X.; Luhman, W.A.; Yagodkin, E.; Holmes, R.J.; Douglas, C.J. Diarylindenotetracenes via a selective cross-coupling/C–H functionalization: Electron donors for organic photovoltaic cells. *Org. Lett.* **2012**, *14*, 1390–1393. [CrossRef]
16. Wegner, H.A.; Scott, L.T.; de Meijere, A. A new Suzuki– Heck-Type coupling cascade: Indeno [1, 2, 3]-annelation of polycyclic aromatic hydrocarbons. *J. Org. Chem.* **2003**, *68*, 883–887. [CrossRef]
17. Pascual, S.; Bour, C.; de Mendoza, P.; Echavarren, A.M. Synthesis of fluoranthenes by hydroarylation of alkynes catalyzed by gold (I) or gallium trichloride. *Beilstein J. Org. Chem.* **2011**, *7*, 1520–1525. [CrossRef]
18. Zhou, J.; Yang, W.; Wang, B.; Ren, H. Friedel–Crafts arylation for the formation of Csp2-Csp2 bonds: A route to unsymmetrical and functionalized polycyclic aromatic hydrocarbons from aryl triazenes. *Angew. Chem., Int. Ed.* **2012**, *51*, 12293–12297. [CrossRef]
19. Reisch, H.A.; Bratcher, M.S.; Scott, L.T. Imposing curvature on a polyarene by intramolecular palladium-catalyzed arylation reactions: A simple synthesis of dibenzo[a,g]corannulene. *Org. Lett.* **2000**, *2*, 1427–1430. [CrossRef]
20. Kawasumi, K.; Mochida, K.; Kajino, T.; Segawa, Y.; Itami, K. Pd(OAc)2/o-Chloranil/M(OTf)n: A catalyst for the direct C–H arylation of polycyclic aromatic hydrocarbons with boryl-, silyl-, and unfunctionalized arenes. *Org. Lett.* **2012**, *14*, 418–421. [CrossRef]
21. Ogawa, N.; Yamaoka, Y.; Yamada, K.-i.; Takasu, K. Synthesis of π-extended fluoranthenes via a KHMDS-promoted anionic-radical reaction cascade. *Org. Lett.* **2017**, *19*, 3327–3330. [CrossRef] [PubMed]

22. Abe, R.; Nagashima, Y.; Tanaka, J.; Tanaka, K. Room Temperature Fluoranthene Synthesis through Cationic Rh(I)/H_8-BINAP-Catalyzed [2+2+2] Cycloaddition: Unexpected Acceleration due to Noncovalent Interactions. *ACS Catal.* **2023**, *13*, 1604–1613. [CrossRef]
23. Wu, Y.-T.; Linden, A.; Siegel, J.S. Formal [(2+ 2)+ 2] and [(2+2)+(2+ 2)] nonconjugated dienediyne cascade cycloadditions. *Org.Lett.* **2005**, *7*, 4353–4355. [CrossRef] [PubMed]
24. Chen, X.; Lu, P.; Wang, Y. Four iodine-mediated electrophilic cyclizations of rigid parallel triple bonds Mapped from 1, 8-Dialkynylnaphthalenes. *Chem.–Eur. J.* **2011**, *17*, 8105–8114. [CrossRef] [PubMed]
25. Quimby, J.M.; Scott, L.T. Expanding the Suzuki–Heck-type coupling cascade: A new indeno [1, 2, 3]-annelation of polycyclic aromatic hydrocarbons. *Adv. Synth. Catal.* **2009**, *351*, 1009–1013. [CrossRef]
26. Yamaguchi, M.; Higuchi, M.; Tazawa, K.; Manabe, K. Three-step synthesis of fluoranthenes through Pd-catalyzed inter-and intramolecular C–H arylation. *J. Org. Chem.* **2016**, *81*, 3967–3974. [CrossRef]
27. Pal, S.; Metin, Ö.; Türkmen, Y.E. Synthesis of fluoranthene derivatives via tandem Suzuki–Miyaura and intramolecular C–H Arylation reactions under both homogeneous and heterogeneous catalytic conditions. *ACS Omega* **2017**, *2*, 8689–8696. [CrossRef]
28. Koutentis, P.A.; Loizou, G.; Lo Re, D. Synthesis of triazafluoranthenones via silver (I)-mediated nonoxidative and oxidative intramolecular palladium-catalyzed cyclizations. *J. Org. Chem.* **2011**, *76*, 5793–5802. [CrossRef]
29. Pathak, S.; Debnath, K.; Pramanik, A. Silica sulfuric acid: A reusable solid catalyst for one pot synthesis of densely substituted pyrrole-fused isocoumarins under solvent-free conditions. *Beilstein J. Org. Chem.* **2013**, *9*, 2344–2353. [CrossRef]
30. Dong, P.; Majeed, K.; Wang, L.; Guo, Z.; Zhou, F.; Zhang, Q. Transition metal-free approach to azafluoranthene scaffolds by aldol condensation/[1+2+3] annulation tandem reaction of isocyanoacetates with 8-(alkynyl)-1-naphthaldehydes. *Chem. Commun.* **2021**, *39*, 4855–4858. [CrossRef]
31. Boraei, A.T.A.; Soliman, S.M.; Haukka, M.; Salama, E.E.; Sopaih, M.; Barakat, A.; Sarhan, A.A.M. Straightforward green synthesis of indeno-furan carboxylates from ninhydrin and β-ketoesters: X-Ray crystal structure, Hirshfeld and DFT investigations. *J. Mol. Struct.* **2022**, *1255*, 132433. [CrossRef]
32. Boraei, A.T.; Ghabbour, H.A.; Sarhan, A.A.; Barakat, A. Expeditious green synthesis of novel 4-methyl-1, 2, 5, 6-tetraazafluoranthen-3 (2H)-one analogue from ninhydrin: N/S-alkylation and aza-Michael addition. *ACS Omega* **2020**, *5*, 5436–5442. [CrossRef] [PubMed]
33. Boraei, A.T.A.; Haukka, M.; Sopaih, M.; Al-Majid, A.M.; Soliman, S.M.; Barakat, A.; Sarhan, A.M. Straightforward One-Pot Synthesis of New 4-Phenyl-1,2,5,6-tetraazafluoranthen-3(2H)-one Derivatives: X-ray Single Crystal Structure and Hirshfeld Analyses. *Crystals* **2022**, *12*, 262. [CrossRef]
34. Rikagu Oxford Diffraction. *CrysAlisPro*; Rikagu Oxford Diffraction Inc.: Yarnton, Oxfordshire, UK, 2020.
35. Sheldrick, G.M. SHELXT–Integrated space-group and crystal-structure determination. *Acta Cryst.* **2015**, *A71*, 3–8. [CrossRef] [PubMed]
36. Sheldrick, G.M. Crystal structure refinement with *SHELXL*. *Acta Cryst.* **2015**, *C71*, 3–8.
37. Hübschle, C.B.; Sheldrick, G.M.; Dittrich, B. ShelXle: A Qt graphical user interface for SHELXL. *J. Appl. Cryst.* **2011**, *44*, 1281–1284. [CrossRef]
38. Turner, M.J.; McKinnon, J.J.; Wolff, S.K.; Grimwood, D.J.; Spackman, P.R.; Jayatilaka, D.; Spackman, M.A. Crystal Explorer17, University of Western Australia. 2017. Available online: https://crystalexplorer.net/ (accessed on 30 July 2020).